

Electronic Supplementary Information

Sensitive structural motifs separately distributed in azide-based 3D EMOFs: A primary explosive with excellent initiation ability and enhanced stability

Yun-Fan Yan,^{a,d} Jian-Gang Xu,^{*a,b,d} Fei Wen,^a Yu Zhang,^a Hong-Yi Bian,^a Bao-Yi Li,^a Ning-Ning Zhang,^c Fa-Kun Zheng^{*a,d} and Guo-Cong Guo^{a,d}

^a State Key Laboratory of Structural Chemistry, Fujian Institute of Research on the Structure of Matter, Chinese Academy of Sciences, Fuzhou, Fujian 350002, P. R. China

^b College of Material Engineering, Fujian Agriculture and Forestry University, Fuzhou, Fujian 350108, P. R. China

^c School of Chemistry and Chemical Engineering, Liaocheng University, Liaocheng, Shandong 252000, P. R. China.

^d Fujian Science & Technology Innovation Laboratory for Optoelectronic Information of China, Fuzhou, Fujian, 350108, P. R. China.

*Corresponding Authors. E-mails: jgxu@fafu.edu.cn, zfk@fjirsm.ac.cn

Index:

- 1. Experimental details.....S3**
- 2. TablesS8**
- 3. Graphics.....S15**
- 4. References.....S24**

1. Experimental details

1.1 Synthesis

Synthesis of $[\text{Cu}_3(\text{N}_3)_4(\text{bmttz})_2]_n$ **1**.

A mixture containing $\text{Hbmttz}\cdot\text{H}_2\text{O}$ (340.8 mg, 1.5 mmol), NaN_3 (97.5 mg, 1.5 mmol) and $\text{Cu}(\text{ClO}_4)_2\cdot 6\text{H}_2\text{O}$ (555.9 mg, 1.5 mmol) was suspended in 7 mL H_2O and sealed in a 20 mL Teflon-lined stainless autoclave and heated at 140 °C for 3 d. The mixture was then rapidly cooled to room temperature. Brown crystalline powder of **1** were obtained after filtration, washed with water and ethanol, and dried in air. Yield: 72% based on $\text{Hbmttz}\cdot\text{H}_2\text{O}$. Anal. Calcd for $\text{C}_8\text{H}_{12}\text{N}_{34}\text{Cu}_3$: C 12.40, H 1.56, N 61.45%. Found: C 12.51, H 1.60, N 62.09%. IR (KBr, cm^{-1}): 2067 vs, 1515 s, 1425 w, 1377 s, 1338 w, 1280 s, 1236 w, 1209 s, 1105 s, 813 s, 763 w, 740 s, 707 s, 669 s, 626 w, 594 s, 513 s (**Fig. S13a**).

Synthesis of $[\text{Cd}_7(\text{N}_3)_{10}(\text{bmttz})_4]_n$ **2**.

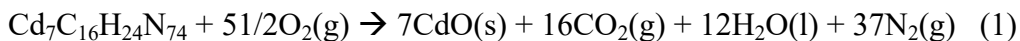
A mixture of $\text{Hbmttz}\cdot\text{H}_2\text{O}$ (113.6 mg, 0.5 mmol), NaN_3 (32.5 mg, 0.5 mmol) and $\text{Cd}(\text{NO}_3)_2\cdot 4\text{H}_2\text{O}$ (154.2 mg, 0.5 mmol) in 5 mL CH_3OH was transferred to a 20 mL Teflon-lined stainless autoclave, held at 160 °C for 4 d, then cooled to room temperature. Colorless flake crystals of **2** were collected by filtration. Yield: 56% based on $\text{Hbmttz}\cdot\text{H}_2\text{O}$. Calcd for $\text{C}_{16}\text{H}_{24}\text{N}_{74}\text{Cd}_7$: C 9.42, H 1.19, N 50.82%. Found: C 9.69, H 1.24 N 49.67%. IR (KBr, cm^{-1}): 3585 s, 3516 s, 2060 vs, 1624 s, 1517 s, 1469 s, 1321 s, 1209 s, 1103 s, 1047 s, 746 s, 727 w, 703 s, 661 s, 615 s (**Fig. S13b**). Relevant crystal data and structural refinement results of **1** and **2** are listed in **Table S1**. Selected bond distances and angles for **1** and **2** are shown in **Table S2**. The pure phases of **1** and **2** are confirmed by PXRD (**Fig. S14**) and elemental analysis.

1.2 Heat of combustion.

The constant volume combustion of the compounds was determined by a precision oxygen bomb calorimeter (5E-AC8018, Changsha Kaiyuan Instrument Co., Ltd., China) based on the Linio-Pyfengdelel-Wsava equation.¹

Before testing, the bomb calorimeter was calibrated by using 1.0 g of certified standard benzoic acid. Then 65.5 mg of the sample was thoroughly mixed with certified standard benzoic acid (calculated: 600.1 mg), and it was lightly pressed to ensure that the mixture could burn stably. Finally, the molded sample is put into a combustion tank to be fully burned in a pure oxygen atmosphere. (Full mixing and compression molding are necessary, otherwise the sample will be directly converted from combustion to detonation, which will not only blow up the support in the combustion tank, but also cause the additive benzoic acid to splash on the inner wall of the tank, resulting in inaccurate test results (**Fig. S6**).

The enthalpy of formation ($\Delta_f H$) is derived from the enthalpy of combustion ($\Delta_c H$). The $\Delta_c H$ value is calculated from $\Delta_c U$ by the gas correction equation: $\Delta_c H = \Delta_c U + \Delta nRT$, where Δn refers to the difference in gas molar amount before and after the combustion process, $R = 8.314 \text{ J}\cdot\text{mol}^{-1}\cdot\text{K}^{-1}$, $T = 298.15 \text{ K}$. The constant volume heat of combustion ($\Delta_c U$) of **2** was measured to be $9.905 \text{ kJ}\cdot\text{g}^{-1}$. The combustion reaction eq 1 in pure oxygen is as follows:



The enthalpy of formation of **2** is obtained by eq 2 as $-4.217 \text{ kJ}\cdot\text{g}^{-1}$ (Hess's law), based on the standard molar enthalpies of formation for known compounds: CdO (s, $-258.35 \text{ kJ}\cdot\text{mol}^{-1}$), CO_2 (g, $-393.51 \text{ kJ}\cdot\text{mol}^{-1}$) and H_2O (l, $-285.83 \text{ kJ}\cdot\text{mol}^{-1}$).

$$\Delta_f H^\circ[\mathbf{2},\text{s}] = 7\Delta_f H^\circ[\text{CdO},\text{s}] + 16\Delta_f H^\circ[\text{CO}_2,\text{g}] + 12\Delta_f H^\circ[\text{H}_2\text{O},\text{l}] - \Delta_c H[\mathbf{2},\text{s}] \quad (2)$$

1.3 Detonation properties

We evaluated the detonation properties of metal-based energetic materials according to the rules of thumb developed by Pang's team and Kamlet's empirical formula. The specific formula is as follows:

$$D = 1.01 \Phi^{1/2} (1 + 1.30\rho) \quad (3)$$

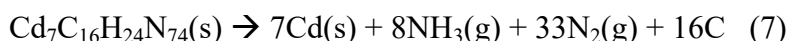
$$P = 1.558 \Phi\rho^2 \quad (4)$$

$$\Phi = 31.68 N(MQ)^{1/2} \quad (5)$$

$$Q = -[\Delta H_f(\text{denotation products}) - \Delta H_f(\text{explosive})]/\text{formula weight of explosive} \quad (6)$$

where D represents detonation velocity ($\text{km}\cdot\text{s}^{-1}$) and P is detonation pressure (GPa), ρ is the density of explosive ($\text{g}\cdot\text{cm}^{-3}$). Φ , N , M and Q are characteristic parameters of an explosive. N is the moles of detonation gases per gram of explosive, M is the average molecular weight of these gases and Q is the heat of detonation ($\text{kcal}\cdot\text{g}^{-1}$).

The ΔH_{det} value of **2** was determined to be $4.397 \text{ kJ}\cdot\text{g}^{-1}$, based on eq 6 with the known $\Delta_f H^\circ$: NH_3 (g, $-46 \text{ kJ}\cdot\text{mol}^{-1}$), H_2O (g, $-241.8 \text{ kJ}\cdot\text{mol}^{-1}$) and the $\Delta_f H^\circ$ value obtained from the above experiment.



For **2**

$$\rho = 2.274 \text{ g}\cdot\text{cm}^{-3}$$

$$Q = \Delta H_{det} = 4.397 \text{ kJ}\cdot\text{g}^{-1} = 1.05 \text{ kcal}\cdot\text{g}^{-1}$$

$$N = 41/2039.89 = 0.02 \text{ mol}\cdot\text{g}^{-1}$$

$$M = (17.034 \times 8 + 28.02 \times 33)/41 = 25.88 \text{ g}\cdot\text{mol}^{-1}$$

$$\Phi = 31.68 \times 0.02 \times (25.88 \times 1.05)^{1/2} = 17.22$$

$$P = 1.558 \times 17.22 \times (2.274)^2 = 26.59 \text{ GPa}$$

$$D = 1.01 \times (17.22)^{1/2} \times (1 + 1.30 \times 2.274) = 7.26 \text{ km}\cdot\text{s}^{-1}$$

1.4 Flame Tests

The small quantities of sample (3 mg) were placed into the Bunsen burner flame with a ladle and the rapid DDT process was observed through the camera. Compound **1** exploded violently under the thermal stimulus to produce the mushroom cloud above the flame with a loud explosion and bright light (**Fig. S7a-c**). By contrast, compound **2** only combusted rapidly under thermal stimulation (**Fig. S7d-f**).

1.5 Sensitivity Tests

The friction and impact sensitivity were determined according to the BAM (German: Bundesanstalt für Materialforschung und Prüfung) standard. Classify the tested compounds with reference to the “UN Recommendations on the Transport of Dangerous Goods”.

Impact sensitivity: The BAM fall hammer measured the impact sensitivities of **1** and **2** according to STANAG 4489 (OZM Research). Free drop a 0.5 kg standard hammer from the set height onto the metal sleeve where the 10 mg sample is placed in. The test results show that the initiation probability of the explosion is about 50%, and the corresponding impact energy are both 1 J. Sensitivity tests show that **1** and **2** are extremely sensitive to shock.²

Friction sensitivity: Friction sensitivity was determined based on STANAG 4487 using a FSKM-10 BAM friction device (manufactured by OZM Research). Experimentally measured friction sensitivities of **1** and **2** are 5 and 20 N, respectively.²

Electrostatic discharge sensitivity: The ESD value of the sample was tested using the OZM research Xpark8 electrostatic spark sensitivity meter, and the discharge energy was obtained based on the formula $E = 0.5 CU^2$. C represents the capacitance of the capacitor in farads (F) and U represents the charging voltage in volts (V). The measured electrostatic spark sensitivity values (E50) at 50% firing rate of **1** and **2** are 40.0 and 30.6 mJ, respectively.

1.6 Initiation capability test

In fact, in the lead plate explosion experiment, the charge density can be adjusted by controlling the charge pressure or the height of the charge column under a certain amount of charge. The charge density is closely related to the detonation effect. We used the commonly used scheme of controlling RDX column height on detonator production line for testing. In consideration of the sensitivities of the compounds are different from that of commercial primary explosives, as well as the high safety risks of suppressing CA-based primers and the limitations of experimental conditions, we cannot strictly follow standard methods to evaluate initiation capabilities. Therefore, according to the reported literatures,^{3,4} we employed the loose charge instead of pressed charge as primary explosive to ignite RDX to evaluate initiation capabilities.

In this test, **1** and **2** were used as primary explosives to fill No. 8 blasting caps (shell diameter: 6.95 mm), and the initiation capability of the samples was evaluated by penetrating the lead plate aperture (thickness: 5 mm). We controlled the height of the RDX grain in the detonator shell by controlling the limit of the punch (weight of 8 kg, 0.8 Mpa). 700 mg RDX was used as a secondary explosive (the first charge: 300 mg RDX pressed into 8 mm high column; the second charge: 300 mg RDX covered on the pressed charge, pressed to a height of 17 mm; the third

charge: 100 mg completely loose RDX). Then a certain amount of primary explosive was spread loosely on the secondary explosive. It was detonated by a pyrotechnical lighter. The hole diameter of the penetrating lead plate was measured by a vernier caliper. Experiments were repeated several times under each charging condition.

2. Tables

Table S1. Crystal data and structure refinement for 1 and 2.

Compound	1	2
<i>CCDC</i>	2162429	2162430
<i>Empirical formula</i>	C ₈ H ₁₂ N ₃₄ Cu ₃	C ₁₆ H ₂₄ N ₇₄ Cd ₇
<i>M_r (g mol⁻¹)</i>	775.14	2039.89
<i>Crystal system</i>	Monoclinic	Orthorhombic
<i>Space group</i>	<i>P2₁/n</i>	<i>Aea2</i>
<i>a/Å</i>	14.1192(4)	18.8663(4)
<i>b/Å</i>	13.1679(3)	28.4894(7)
<i>c/Å</i>	15.5670(4)	11.0875(3)
<i>α°</i>	90	90
<i>β°</i>	96.425(3)	90
<i>γ°</i>	90	90
<i>V/Å³</i>	2876.04(13)	5959.4(3)
<i>D_c/g cm⁻³</i>	1.790	2.274
<i>Temperature (K)</i>	100(2)	100(10)
<i>F(000)</i>	1540	3896
<i>GOF on F²</i>	1.048	1.059
<i>R_I (I > 2σ(I))^a</i>	0.0484	0.0325
<i>wR₂ (I > 2σ(I))^b</i>	0.1295	0.0861
<i>R_I (all data)^a</i>	0.0618	0.0356
<i>wR₂ (all data)^b</i>	0.1391	0.0874

^a $R_1 = \sum(F_o - F_c)/\sum F_o$; ^b $wR_2 = [\sum w(F_o^2 - F_c^2)^2/\sum w(F_o^2)^2]^{1/2}$.

Table S2. Selected bond distances (Å) and bond angles (°) for 1 and 2.

Compound 1			
Cu(1)–N(102)	1.997(3)	Cu(1)–N(11)	2.001(3)
Cu(1)–N(207)#2	2.011(3)	Cu(1)–N(41)#2	2.255(3)
Cu(1)–N(11)#3	1.992(3)	N(11)–Cu(1)#3	1.992(3)
N(207)–Cu(1)#4	2.011(3)	N(41)–Cu(1)#4	2.255(3)
Cu(2)–N(21)	1.986(3)	Cu(2)–N(111)	1.981(3)
Cu(2)–N(31)	2.023(3)	Cu(2)–N(202)	1.993(3)
Cu(3)–N(211)	2.008(3)	Cu(3)–N(41)	1.979(3)
Cu(3)–N(31)#4	2.050(3)	Cu(3)–N(21)#4	2.037(3)
Cu(3)–N(110)#5	2.322(3)	N(110)–Cu(3)#1	2.322(3)
N(31)–Cu(3)#2	2.050(3)	N(21)–Cu(3)#2	2.037(3)
N(207)#2–Cu(1)–N(41)#2	93.35(12)	N(103)–N(102)–Cu(1)	124.9(2)
N(101)–N(102)–Cu(1)	122.1(2)	N(11)#3–Cu(1)–N(102)	93.99(13)
N(11)#3–Cu(1)–N(11)	79.55(15)	N(102)–Cu(1)–N(11)	167.92(13)
N(11)#3–Cu(1)–N(207)#2	159.20(14)	N(102)–Cu(1)–N(207)#2	91.36(13)
N(11)–Cu(1)–N(207)#2	91.32(13)	N(11)#3–Cu(1)–N(41)#2	106.81(13)
N(102)–Cu(1)–N(41)#2	88.93(12)	N(11)–Cu(1)–N(41)#2	102.66(13)
N(12)–N(11)–Cu(1)	124.9(3)	Cu(1)#3–N(11)–Cu(1)	100.45(15)
N(12)–N(11)–Cu(1)#3	129.5(3)	C(23)–N(207)–Cu(1)#4	132.5(3)

N(206)–N(207)–Cu(1)#4	113.4(2)	N(42)–N(41)–Cu(1)#4	119.2(3)
Cu(3)–N(41)–Cu(1)#4	114.82(15)	N(111)–Cu(2)–N(21)	170.31(13)
N(111)–Cu(2)–N(202)	89.43(13)	N(21)–Cu(2)–N(202)	94.32(13)
N(111)–Cu(2)–N(31)	95.52(13)	C(13)–N(111)–Cu(2)	121.8(2)
N(21)–Cu(2)–N(31)	81.31(13)	N(110)–N(111)–Cu(2)	130.3(2)
N(202)–Cu(2)–N(31)	174.06(12)	N(32)–N(31)–Cu(2)	116.6(2)
N(203)–N(202)–Cu(2)	123.7(2)	N(201)–N(202)–Cu(2)	123.1(3)
N(22)–N(21)–Cu(2)	119.2(2)	Cu(2)–N(31)–Cu(3)#2	97.79(13)
Cu(2)–N(21)–Cu(3)#2	99.43(15)	N(41)–Cu(3)–N(211)	91.63(14)
N(41)–Cu(3)–N(21)#4	96.89(13)	N(211)–Cu(3)–N(21)#4	163.77(12)
N(41)–Cu(3)–N(31)#4	172.51(13)	N(211)–Cu(3)–N(31)#4	90.42(12)
N(21)#4–Cu(3)–N(31)#4	79.47(11)	N(41)–Cu(3)–N(110)#5	95.54(12)
N(211)–Cu(3)–N(110)#5	105.55(11)	N(21)#4–Cu(3)–N(110)#5	87.43(12)
N(31)#4–Cu(3)–N(110)#5	90.85(11)	C(23)–N(211)–Cu(3)	129.9(3)
N(210)–N(211)–Cu(3)	122.6(2)	N(42)–N(41)–Cu(3)	118.9(3)
N(32)–N(31)–Cu(3)#2	119.0(2)	N(22)–N(21)–Cu(3)#2	119.6(3)
N(109)–N(110)–Cu(3)#1	129.9(2)	N(111)–N(110)–Cu(3)#1	119.1(2)
Compound 2			
Cd(1)–N(101)	2.355(8)	Cd(1)–N(111)	2.366(7)
Cd(1)–N(31)	2.498(8)	Cd(1)–N(202)	2.366(8)

Cd(1)–N(83)#1	2.392(7)	Cd(1)–N(53)#4	2.391(8)
Cd(1)–N(106)	2.581(8)	Cd(2)–N(110)	2.356(7)
Cd(2)–N(71)#3	2.327(8)	Cd(2)–N(51)	2.341(8)
Cd(2)–N(31)	2.448(8)	Cd(2)–N(41)	2.252(8)
Cd(2)–N(61)	2.274(7)	N(71)–Cd(2)#6	2.327(8)
Cd(3)–N(71)	2.278(8)	Cd(3)–N(51)#6	2.372(8)
Cd(3)–N(81)	2.336(8)	Cd(3)–N(207)#7	2.454(7)
Cd(3)–N(61)	2.248(7)	Cd(3)–N(205)#7	2.430(7)
N(205)–Cd(3)#2	2.430(7)	N(207)–Cd(3)#2	2.454(7)
N(51)–Cd(3)#3	2.372(8)	Cd(4)–N(211)#6	2.380(8)
Cd(4)–N(206)#6	2.550(7)	Cd(4)–N(211)#5	2.380(8)
Cd(4)–N(206)#5	2.550(7)	Cd(4)–N(201)#6	2.596(7)
Cd(4)–N(201)#5	2.596(7)	Cd(4)–N(83)	2.347(7)
Cd(4)–N(83)#8	2.347(7)	N(206)–Cd(4)#1	2.550(7)
N(211)–Cd(4)#1	2.380(8)	N(201)–Cd(4)#1	2.596(7)
N(101)–Cd(1)–N(111)	126.6(3)	N(101)–Cd(1)–N(202)	89.3(3)
N(101)–Cd(1)–N(31)	156.8(3)	N(101)–Cd(1)–N(83)#1	81.7(3)
N(101)–Cd(1)–N(53)#4	91.2(3)	N(111)–Cd(1)–N(106)	63.3(3)
N(101)–Cd(1)–N(106)	63.5(3)	N(31)–Cd(1)–N(106)	139.2(3)
N(111)–Cd(1)–N(31)	76.4(3)	N(202)–Cd(1)–N(111)	98.7(3)

N(111)–Cd(1)–N(83)#1	151.1(3)	N(202)–Cd(1)–N(31)	88.5(3)
N(111)–Cd(1)–N(53)#4	87.8(3)	N(202)–Cd(1)–N(83)#1	85.6(3)
N(202)–Cd(1)–N(53)#4	171.5(3)	N(53)#4–Cd(1)–N(31)	87.8(3)
N(202)–Cd(1)–N(106)	103.2(3)	N(53)#4–Cd(1)–N(83)#1	86.0(3)
N(83)#1–Cd(1)–N(31)	75.2(3)	N(53)#4–Cd(1)–N(106)	84.6(3)
N(83)#1–Cd(1)–N(106)	143.6(3)	C(12)–N(101)–Cd(1)	118.4(6)
N(102)–N(101)–Cd(1)	135.6(6)	C(13)–N(111)–Cd(1)	117.7(6)
N(110)–N(111)–Cd(1)	135.4(6)	N(32)–N(31)–Cd(1)	121.6(5)
N(203)–N(202)–Cd(1)	133.3(6)	N(201)–N(202)–Cd(1)	114.5(5)
N(105)–N(106)–Cd(1)	122.8(6)	N(107)–N(106)–Cd(1)	122.2(6)
N(52)–N(53)–Cd(1)#4	123.8(6)	Cd(4)–N(83)–Cd(1)#5	123.5(3)
N(82)–N(83)–Cd(1)#5	118.7(6)	N(110)–Cd(2)–N(31)	81.0(2)
Cd(2)–N(31)–Cd(1)	120.2(3)	N(71)#3–Cd(2)–N(110)	87.4(3)
N(41)–Cd(2)–N(51)	89.4(3)	N(71)#3–Cd(2)–N(51)	78.9(3)
N(41)–Cd(2)–N(31)	85.0(3)	N(71)#3–Cd(2)–N(31)	90.3(3)
N(41)–Cd(2)–N(61)	94.2(3)	N(51)–Cd(2)–N(110)	164.2(2)
N(61)–Cd(2)–N(110)	92.6(3)	N(51)–Cd(2)–N(31)	91.1(3)
N(61)–Cd(2)–N(71)#3	91.8(3)	N(41)–Cd(2)–N(110)	103.5(3)
N(61)–Cd(2)–N(51)	95.6(3)	N(41)–Cd(2)–N(71)#3	167.3(3)
N(61)–Cd(2)–N(31)	173.2(3)	N(109)–N(110)–Cd(2)	127.1(6)
N(32)–N(31)–Cd(2)	116.3(6)	N(42)–N(41)–Cd(2)	123.6(6)

N(62)–N(61)–Cd(2)	115.1(6)	N(52)–N(51)–Cd(2)	125.8(6)
N(111)–N(110)–Cd(2)	121.2(5)	Cd(3)–N(61)–Cd(2)	128.8(3)
Cd(2)–N(51)–Cd(3)#3	98.9(3)	Cd(3)–N(71)–Cd(2)#6	102.1(3)
N(72)–N(71)–Cd(2)#6	118.3(6)	N(205)#7–Cd(3)–N(207)#7	53.0(2)
N(61)–Cd(3)–N(81)	91.9(3)	N(71)–Cd(3)–N(205)#7	102.2(3)
N(61)–Cd(3)–N(207)#7	98.7(3)	N(71)–Cd(3)–N(51)#6	79.3(3)
N(71)–Cd(3)–N(81)	107.5(3)	N(61)–Cd(3)–N(205)#7	87.7(3)
N(71)–Cd(3)–N(207)#7	148.4(3)	N(61)–Cd(3)–N(71)	99.5(3)
N(51)#6–Cd(3)–N(205)#7	98.5(3)	N(61)–Cd(3)–N(51)#6	173.8(3)
N(51)#6–Cd(3)–N(207)#7	85.1(2)	N(72)–N(71)–Cd(3)	137.6(6)
N(81)–Cd(3)–N(205)#7	150.0(3)	N(82)–N(81)–Cd(3)	126.9(6)
N(81)–Cd(3)–N(51)#6	82.8(2)	N(62)–N(61)–Cd(3)	114.3(6)
N(81)–Cd(3)–N(207)#7	97.5(3)	N(206)–N(207)–Cd(3)#2	96.4(5)
N(206)–N(205)–Cd(3)#2	97.4(5)	C(23)–N(207)–Cd(3)#2	154.7(6)
C(22)–N(205)–Cd(3)#2	154.4(6)	N(52)–N(51)–Cd(3)#3	123.8(6)
N(206)#5–Cd(4)–N(206)#6	124.8(3)	N(206)#5–Cd(4)–N(201)#5	61.6(2)
N(206)#6–Cd(4)–N(201)#5	137.3(2)	N(206)#5–Cd(4)–N(201)#6	137.3(2)
N(211)#5–Cd(4)–N(206)#6	80.8(2)	N(206)#6–Cd(4)–N(201)#6	61.6(2)
N(211)#6–Cd(4)–N(206)#5	80.8(2)	N(211)#5–Cd(4)–N(201)#6	77.9(2)
N(211)#5–Cd(4)–N(206)#5	63.7(2)	N(211)#5–Cd(4)–N(201)#5	125.0(2)
N(211)#6–Cd(4)–N(206)#6	63.7(2)	N(211)#6–Cd(4)–N(201)#5	77.9(2)

N(211)#6–Cd(4)–N(211)#5	98.7(4)	N(211)#6–Cd(4)–N(201)#6	125.0(2)
N(201)#6–Cd(4)–N(201)#5	147.5(3)	N(83)#8–Cd(4)–N(206)#6	139.0(2)
N(83)–Cd(4)–N(206)#5	139.0(2)	N(83)–Cd(4)–N(206)#6	81.0(2)
N(83)#8–Cd(4)–N(206)#5	81.0(2)	N(83)–Cd(4)–N(211)#5	157.2(3)
N(83)–Cd(4)–N(211)#6	85.4(3)	N(83)–Cd(4)–N(201)#5	77.8(2)
N(83)#8–Cd(4)–N(211)#6	157.2(3)	N(83)–Cd(4)–N(201)#6	81.4(2)
N(83)–Cd(4)–N(211)#6	85.4(3)	N(83)#8–Cd(4)–N(201)#5	81.4(2)
N(83)#8–Cd(4)–N(201)#6	77.8(2)	N(82)–N(83)–Cd(4)	117.0(6)
N(83)–Cd(4)–N(83)#8	99.6(4)	N(205)–N(206)–Cd(4)#1	124.6(5)
N(207)–N(206)–Cd(4)#1	122.2(5)	N(210)–N(211)–Cd(4)#1	135.9(6)
C(23)–N(211)–Cd(4)#1	117.8(6)	N(202)–N(201)–Cd(4)#1	127.9(5)
C(22)–N(201)–Cd(4)#1	109.4(5)		

Symmetry codes for compounds **1** and **2**, For **1**, #1 $-x + 1/2, y + 1/2, -z + 3/2$. #2 $x + 1/2, -y + 3/2, z - 1/2$. #3 $-x + 1, -y + 2, -z$. #4 $x - 1/2, -y + 3/2, z + 1/2$. #5 $-x + 1/2, y - 1/2, -z + 3/2$. For **2**, #1 $x - 1/2, -y + 1, z + 1/2$. #2 $x, y, z + 1$. #3 $-x + 3/2, y, z + 1/2$. #4 $-x + 1, -y + 1, z$. #5 $x + 1/2, -y + 1, z - 1/2$. #6 $-x + 3/2, y, z - 1/2$. #7 $x, y, z - 1$. #8 $-x + 2, -y + 1, z$.

3. Graphics

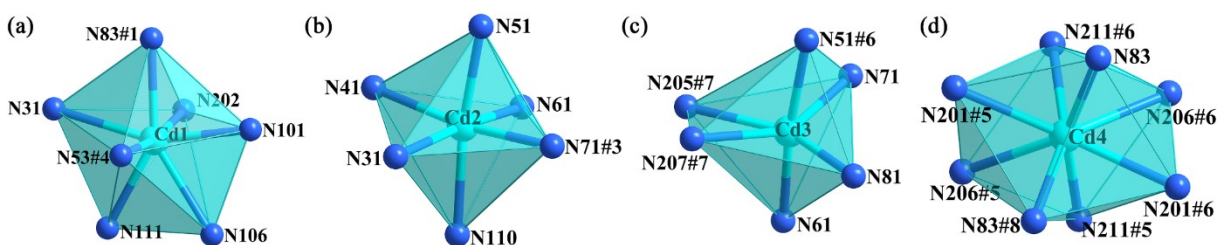


Fig. S1 (a) The coordination environment of Cd1 atom of **2**. (b) The coordination environment of Cd2 atom of **2**. (c) The coordination environment of Cd3 atom of **2**. (d) The coordination environment of Cd4 atom of **2**.

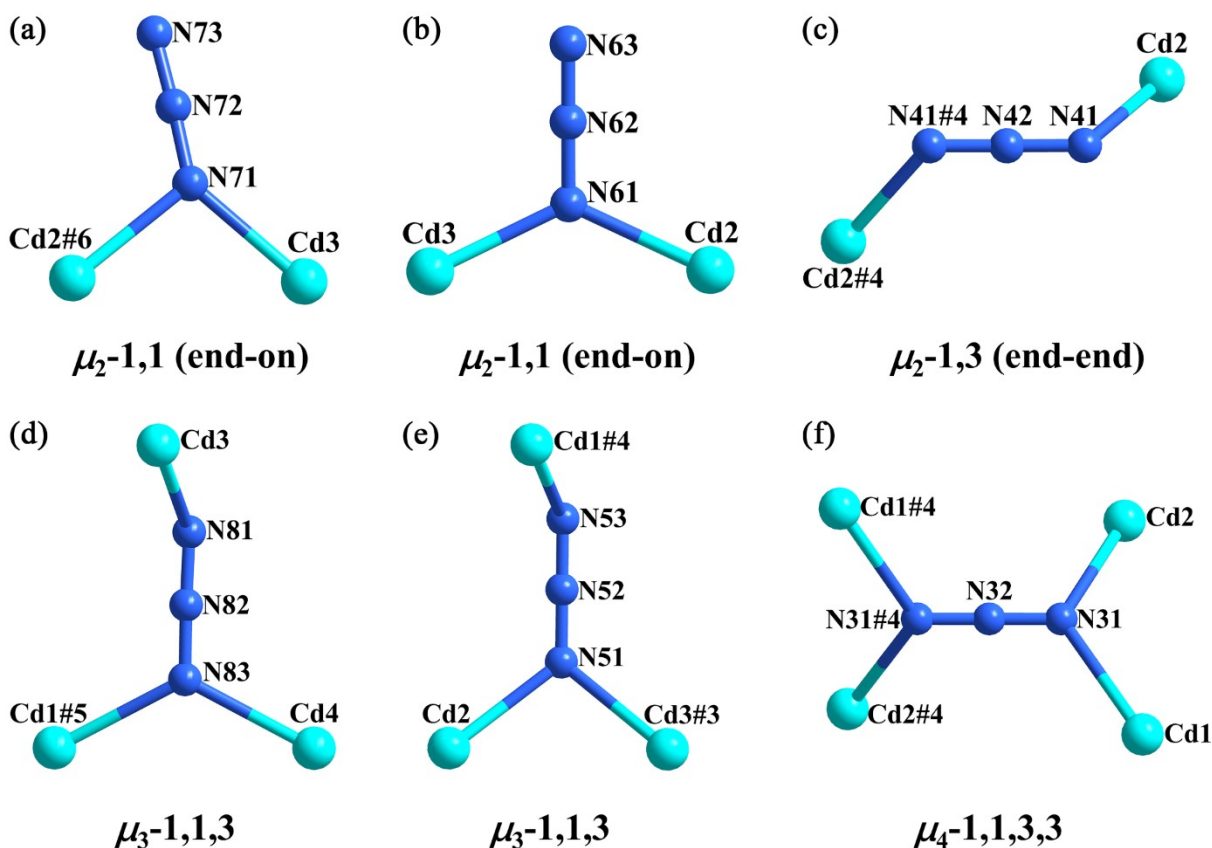


Fig. S2 The coordination environments of N_3^- anions of **2**. (a) μ_2 -1,1 (end-on) bridge mode. (b) μ_2 -1,1 (end-on) bridge mode. (c) μ_2 -1,3 (end-end) bridge mode. (d) μ_3 -1,1,3 bridge mode. (e) μ_3 -1,1,3 bridge mode. (f) μ_4 -1,1,3,3 bridge mode. Symmetry codes: #1 $x - 1/2, -y + 1, z + 1/2$. #2 $x,$

$y, z + 1$. #3 $-x + 3/2, y, z + 1/2$. #4 $-x + 1, -y + 1, z$. #5 $x + 1/2, -y + 1, z - 1/2$. #6 $-x + 3/2, y, z - 1/2$. #7 $x, y, z - 1$. #8 $-x + 2, -y + 1, z$.

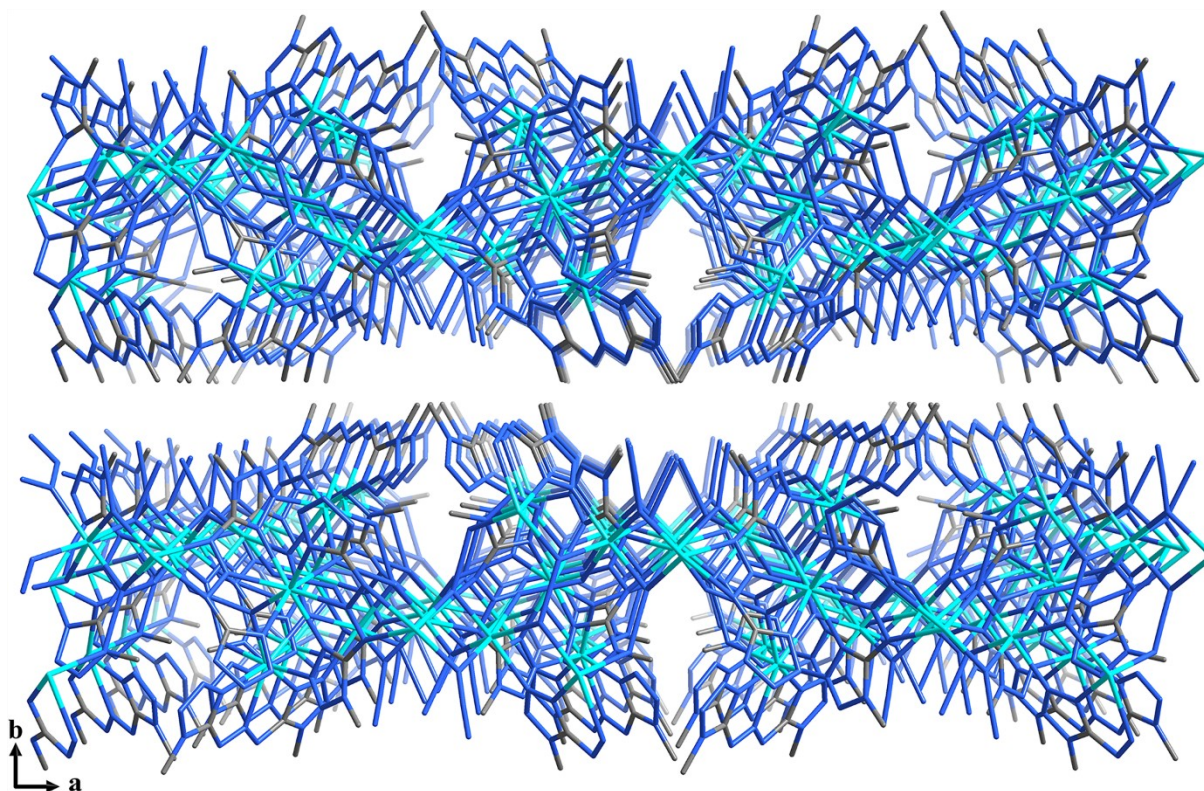


Fig. S3 The 3D supramolecular structure of **2**.

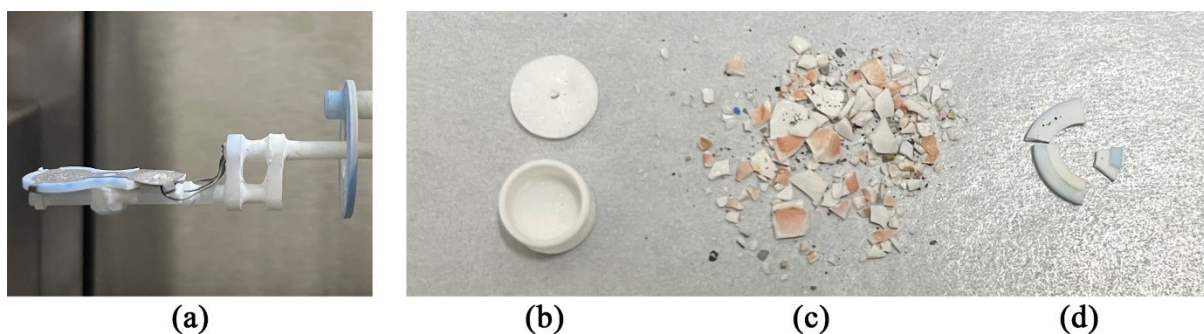


Fig. S4 (a) The damaged sample stage after completion of TGA-DSC test. (b) The alumina crucible before the TGA-DSC test. (c) The shape of alumina crucible after the TGA-DSC test. (d) The fragments of the sample stage after TGA-DSC test.

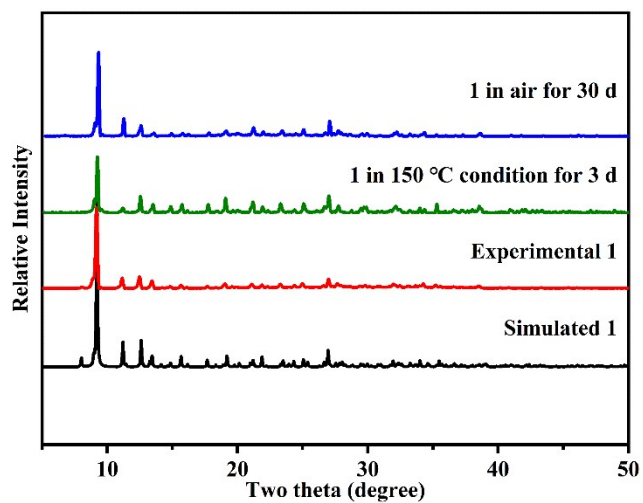


Fig. S5 The PXRD patterns of the simulated **1**, the as-synthesized **1**, compound **1** in 150 °C condition for 3 d, compound **1** in air for 30 d.



Fig. S6 (a) The complete oxygen bomb. (b) The Oxygen bomb destroyed by explosion.

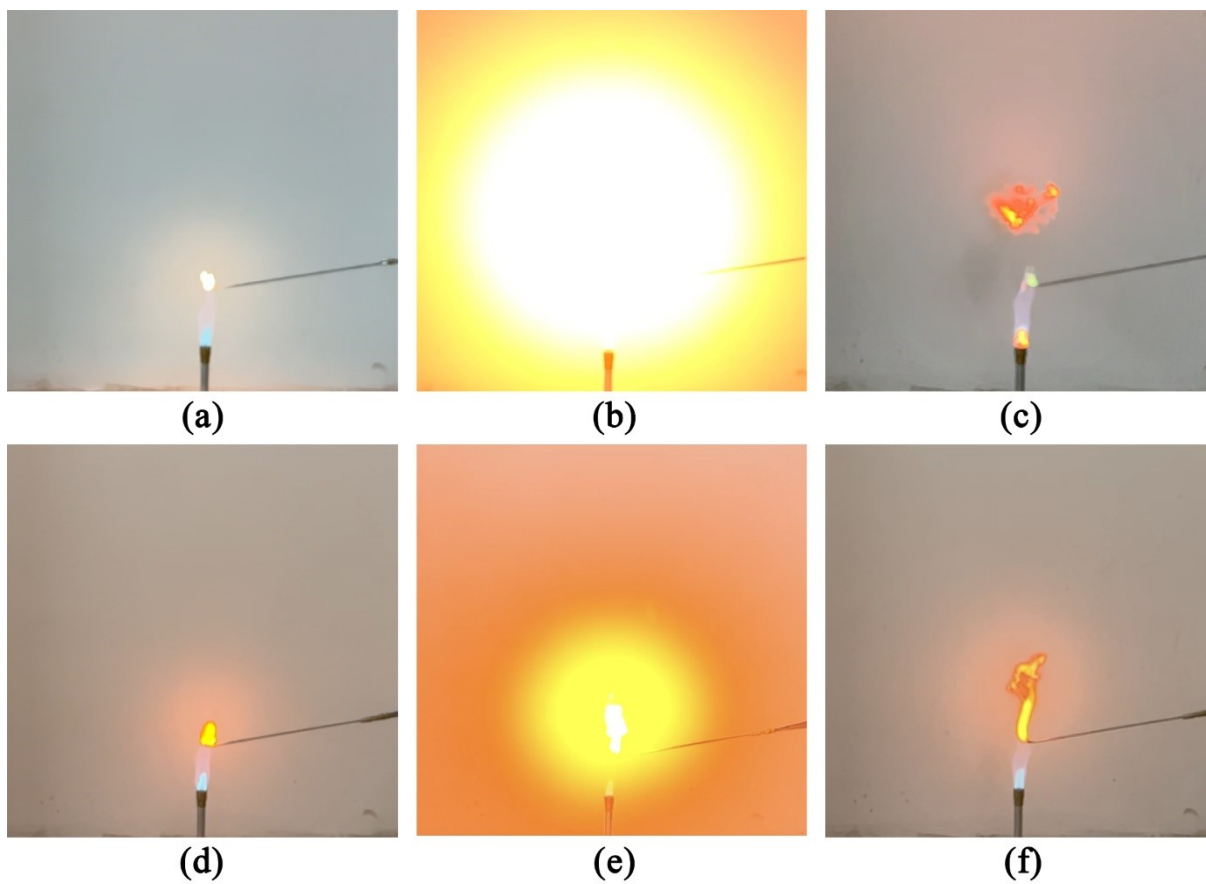


Fig. S7 Flame test for **1**: (a) The igniting moment. (b) The bright light produced by explosion. (c) A mushroom cloud created by explosion. Flame test for **2**: (d) The igniting moment. (e) The light created by rapid combustion. (f) The flame produced by rapid combustion.

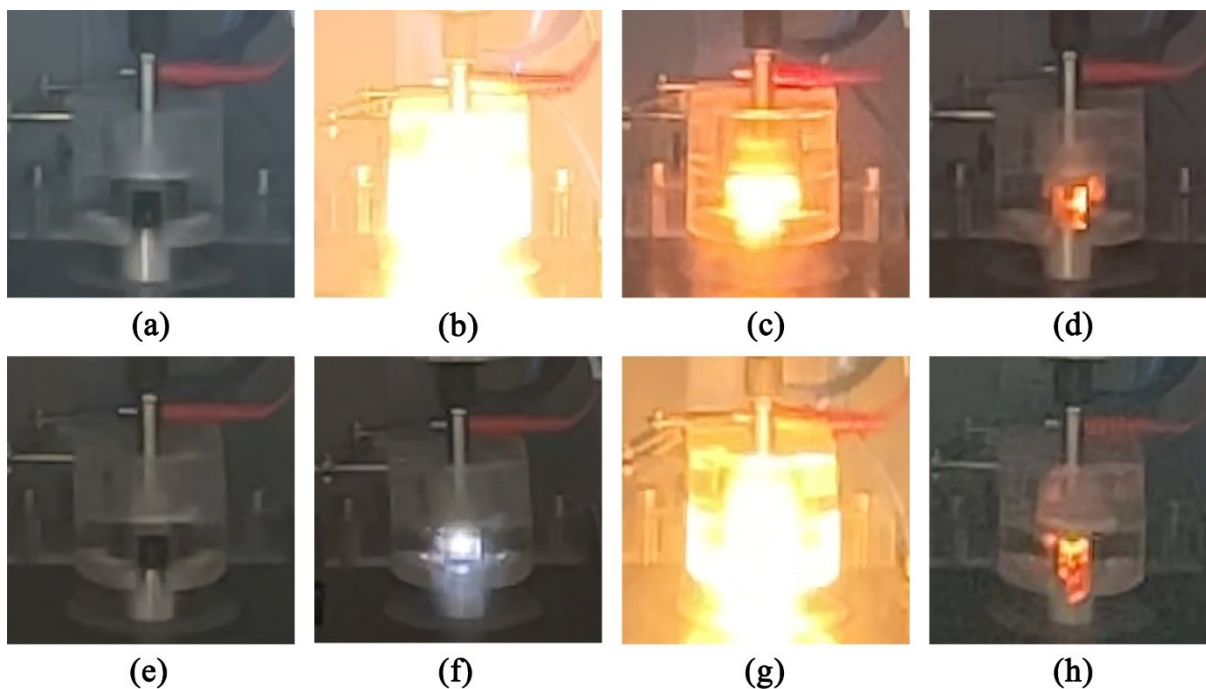


Fig. S8 The electrical spark sensitivity test for **1**: (a) Before electrical spark sensitivity test. (b) At the moment of detonation. (c) In the middle of electrical spark sensitivity test. (d) At the moment of detonation near the end. The electrical spark sensitivity test for **2**: (e) Before electrical spark sensitivity test. (f) At the moment of detonation. (g) In the middle of electrical spark sensitivity test. (h) At the moment of detonation near the end.

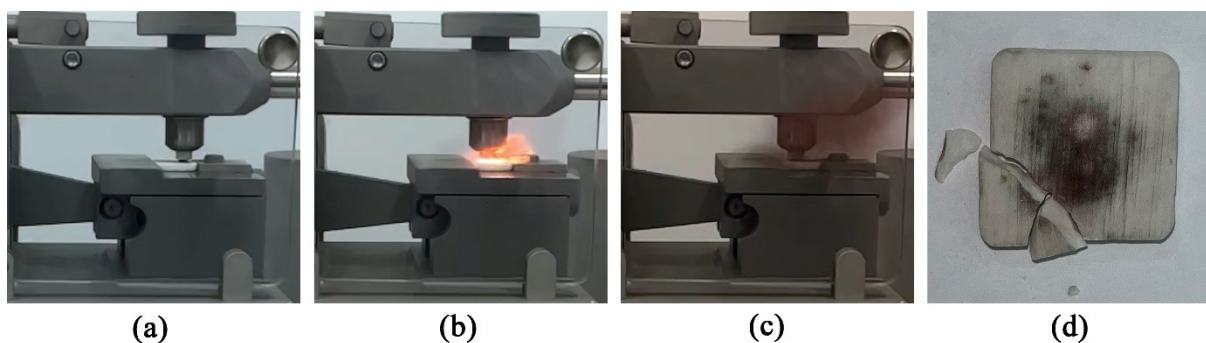


Fig. S9 Friction sensitivity test of **1**. (a) 10 mg of sample placed on a special porcelain plate. (b) The violent explosion in FS test. (c) After FS test. (d) Cracked porcelain plate after FS test.

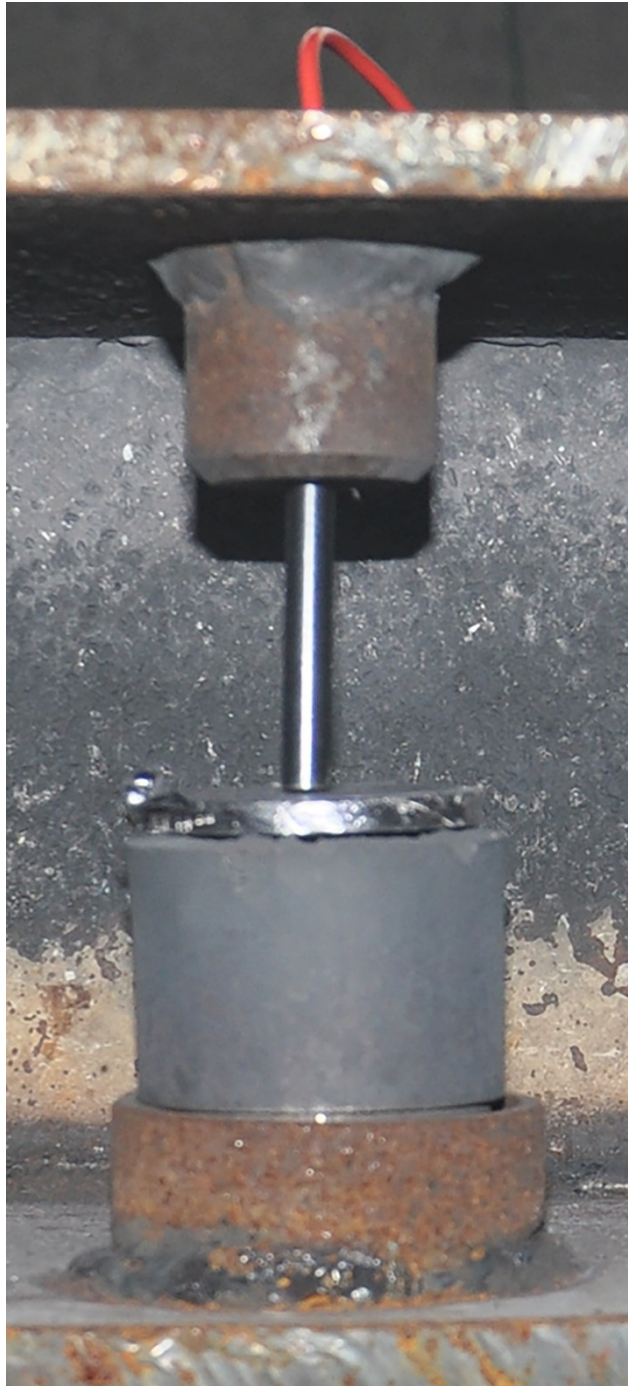


Fig. S10 Real shot of the setup of the lead plate explosive test.

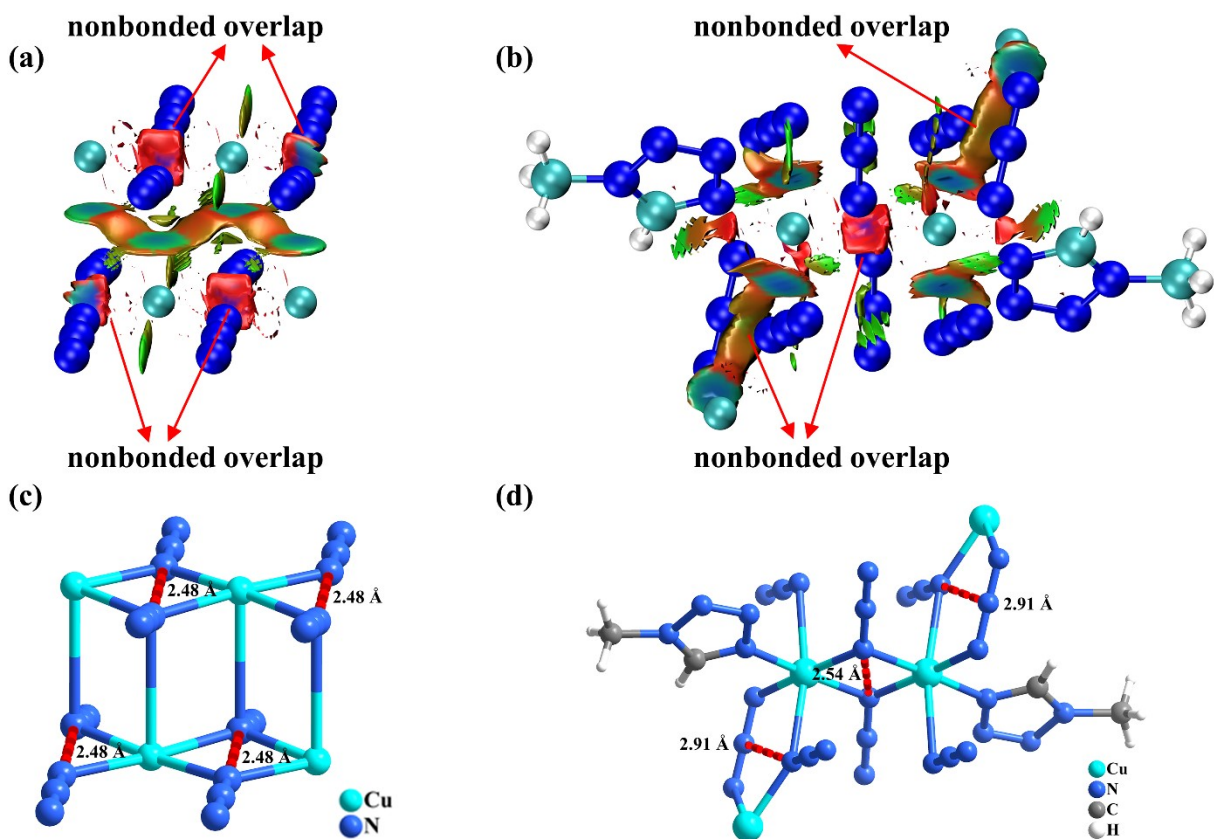


Fig. S11 Gradient isosurfaces of CA (a) and Cu-MTZ (b). The N...N distances with strong repulsive steric clashes for CA (c) and Cu-MTZ (d).

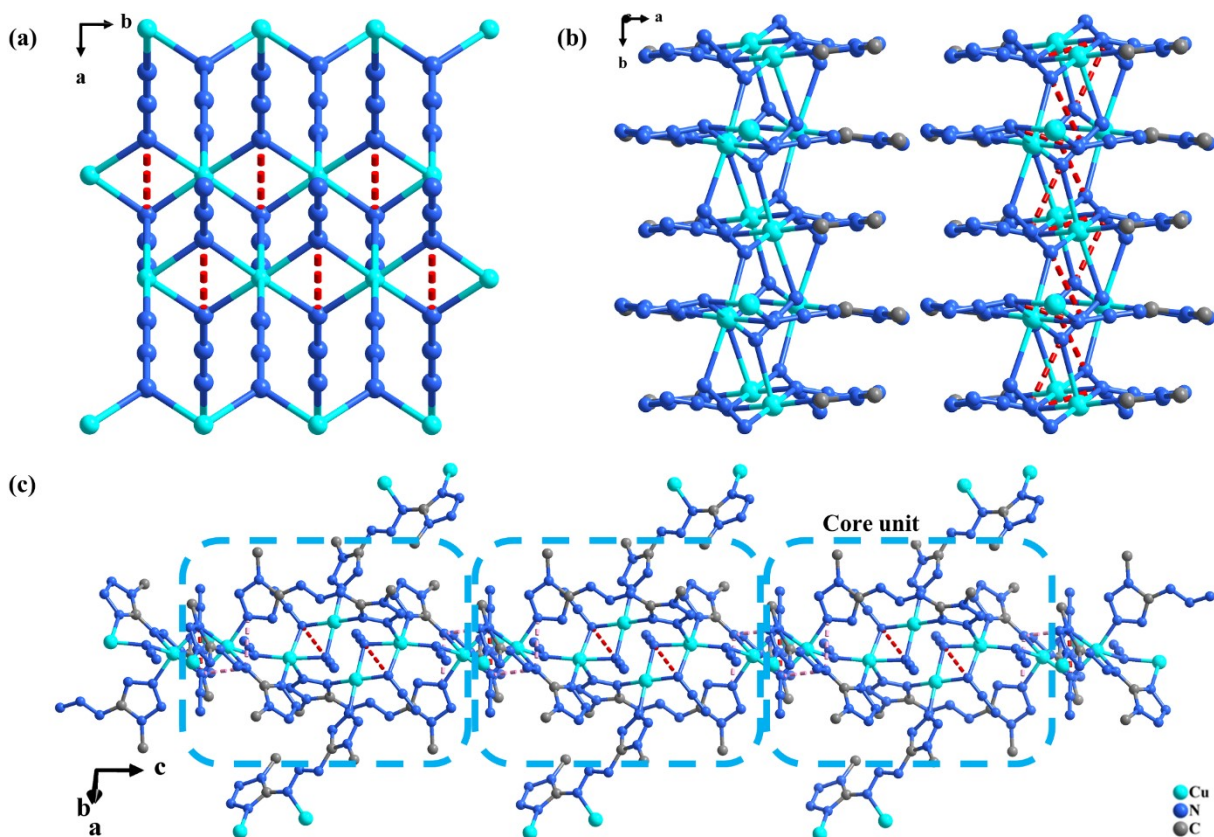


Fig. S12 (a) The 3D structure of CA. (b) The 2D layered structure of Cu-MTZ. (c) The core units of **1** extend infinitely along the *c*-axis. The locations where strong repulsive steric clashes exist are indicated by dashed lines.

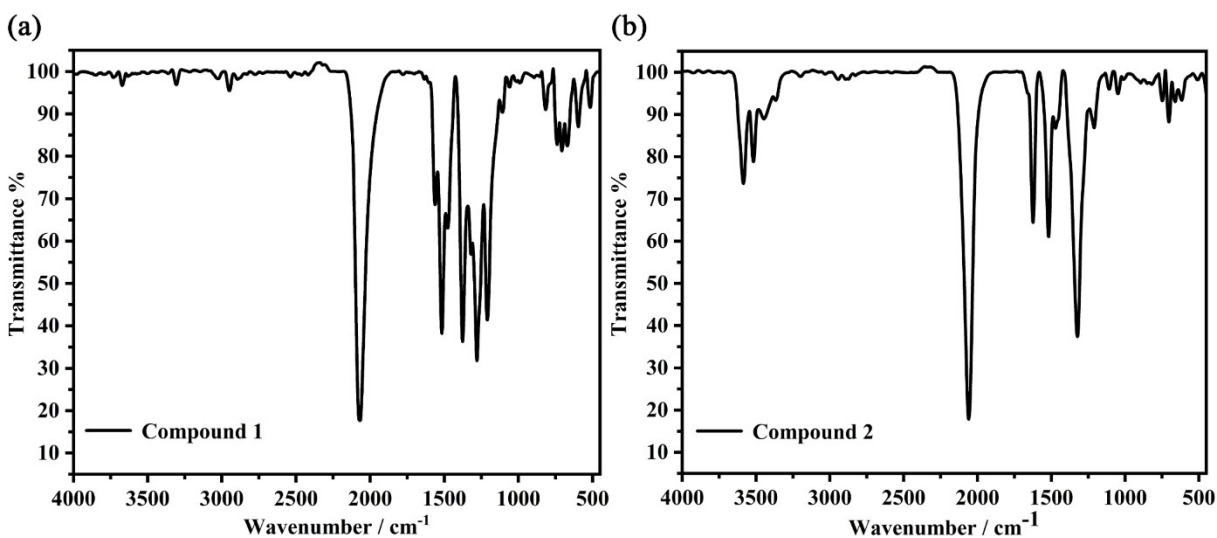


Fig. S13 (a) The IR spectra of **1**. (b) The IR spectra of **2**.

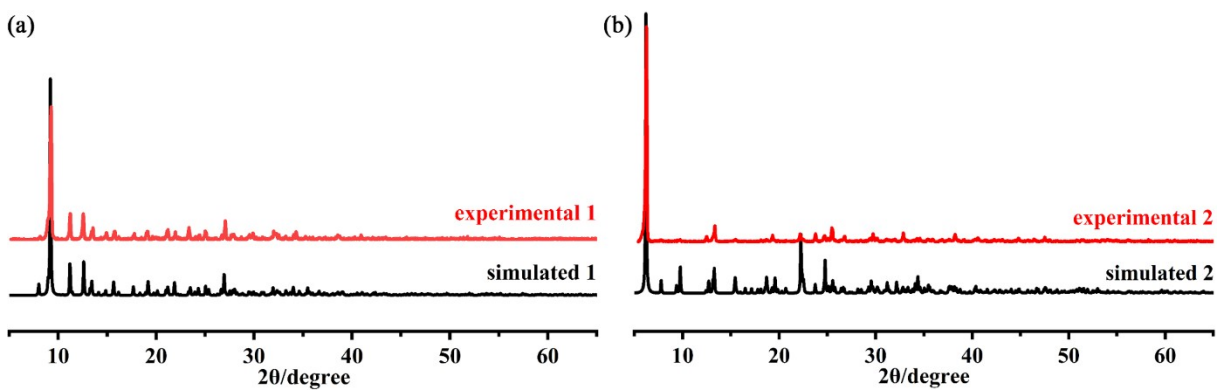


Fig. S14 (a) The powdered *X*-ray diffraction (PXRD) pattern of **1**. (b) The PXRD pattern of **2**.

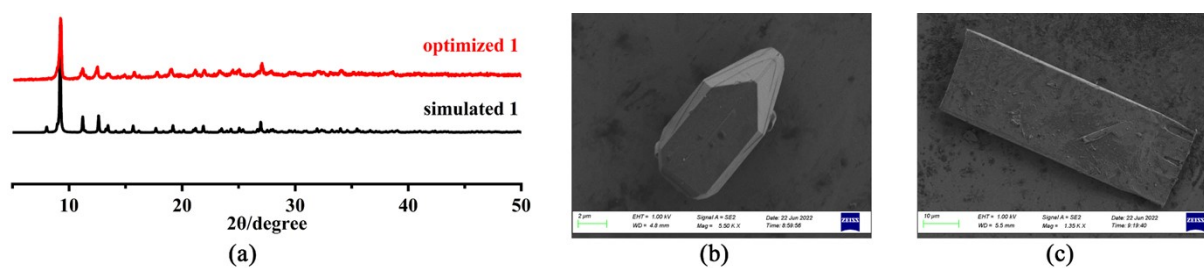


Fig. S15 (a) The powdered *X*-ray diffraction (PXRD) pattern of optimized **1**. (b) The morphology of **1** recorded by FE-SEM. (c) The morphology of **2** recorded by FE-SEM.

4. References

- [1] Popov, M. M. Thermometry and Calorimetry; Moscow University Publishing House: Moscow. **1954**, 382.
- [2] Impact: insensitive > 40 J, less sensitive ≥ 35 J, sensitive ≥ 4 J, very sensitive ≤ 3 J; Friction: insensitive > 360 N, less sensitive $= 360$ N, 80 N $<$ sensitive < 360 N, very sensitive ≤ 80 N, extremely sensitive ≤ 10 N.
- [3] M. H. H. Wurzenberger, M. Lommel, M. S. Gruhne, N. Szimhardt, J. Stierstorfer, Refinement of Copper(II) Azide with 1-Alkyl-5H-tetrazoles: Adaptable Energetic Complexes, *Angew. Chem., Int. Ed.*, 2020, **59**, 1–5.
- [4] T. M. Klapötke, M. Kofen, J. Stierstorfer, N-Functionalisation of 5,5'-bistetrazole providing 2,2'-di(azidomethyl)bistetrazole: a melt-castable metal-free green primary explosive, *Dalton Trans.*, 2021, **39**, 13656-13660.